THE ASTROPHYSICAL JOURNAL, 395:130–139, 1992 August 10

INTERSTELLAR DUST FROM THE MILKY WAY TO THE MAGELLANIC CLOUDS

YICHUAN C. PEI
Princeton University Observatory, Peyton Hall, Princeton, NJ 08544
Received 1991 November 22; accepted 1992 February 13

ABSTRACT

Interstellar dust in the Magellanic Clouds, with a weak or nearly absent 2175 Å extinction feature, may be of interest in studies of galaxies in early stages of chemical evolution. To this inquiry, we extend the graphite-silicate grain model, introduced by Mathis, Rumpl, & Nordsieck and developed by Draine & Lee, from the Milky Way to the Magellanic Clouds. We find that the empirical extinction curves in the Large and Small Magellanic Clouds can be reproduced by adjusting only the relative abundances of graphite and silicate grains, while leaving all other model properties fixed to those appropriate for the Galactic extinction curve. Using the graphite-silicate models, we calculate the absorption and scattering optical depths, the mass-density ratio of interstellar dust to neutral hydrogen, and the Kramers-Kronig relation for all three galaxies. We also present a fitting function for the three extinction curves, valid not only over the observed range of wavelengths but also over the full range as predicted by the models. All the quantities we derived here are independent of the dust-to-gas ratios in the Milky Way and the Magellanic Clouds, and can be applied to other galaxies if they contain Galactic or Magellanic-type dust.

Subject headings: dust, extinction — galaxies: ISM — intergalactic medium — Magellanic Clouds

1. INTRODUCTION

The Milky Way and the Large and Small Magellanic Clouds (GAL, LMC, and SMC) are the only three galaxies with observed interstellar extinction curves. Extensive measurements exist along hundreds of lines of sight in the Milky Way (Savage & Mathis 1979), and some but less extensive measurements are also available along tens of lines of sight in the LMC and SMC (Fitzpatrick 1989). Empirically, the average extinction curves over the range of ultraviolet wavelengths display substantial and significant variations from one galaxy to another. The most conspicuous difference is the sequential changes in the strength of the 2175 Å feature and the level of the far-ultraviolet extinction from the Milky Way to the LMC to the SMC: the former decreases, while the latter increases. It is generally thought that variations in the extinction curve are caused by some evolution in the size distribution and/or chemical composition of dust grains. The different empirical extinction curves in the Milky Way, LMC, and SMC would imply different optical and physical properties of grains. Although grain properties are not uniquely determined from the extinction alone, the extinction curve, when interpreted through dust models, still provides the most indicative information about the optical and physical properties of interstellar dust grains. Unfortunately, such information has only been derived for Galactic-type dust and is not available for Magellanic-type dust.

Magellanic-type dust is interesting for several reasons. The Magellanic Clouds have lower abundances of heavy elements and dust than the Milky Way. In this respect, they may resemble galaxies at high redshifts, which are presumably in early stages of the chemical enrichment. There is some evidence for this from the recent detection of reddening in the damped Lyα systems discovered in the spectra of quasars. The damped Lyα systems contain most of the neutral hydrogen in the universe at redshifts $2 \lesssim z \lesssim 3$ and are generally thought to be the high-redshift analogs or progenitors of present-day galactic disks (see Wolfe 1990 for a review). The detection of reddening, combined with the absence of strong excess extinction centered near 2175 Å in several damped Lyα systems, indicates that the shape of the extinction curve in the damped Lyα systems is similar to that in the LMC or SMC rather than that in the Milky Way (Pei, Fall, & Bechtold 1991, and references therein). The estimates of the typical dust-to-gas ratio in the damped Lyα systems are then about one order of magnitude lower than that in the Milky Way. It is valuable, therefore, to provide the optical and physical properties of interstellar grains appropriate not only for Galactic-type dust but also for LMC and SMC-type dust. Together, they should cover a wide range of possibilities, on which many studies of dust at high redshifts could be based empirically.

In this paper, we extend the standard interstellar dust model with a mixture of pure graphite and silicate grains from the Milky Way to the LMC to the SMC. Our approach is to examine the consequences of varying the graphite-to-silicate ratios in the model, and our goal is to provide a plausible range in the optical and physical properties that are self-consistent with the empirical extinction curves in the three galaxies. The graphite-silicate model, as originally proposed by Mathis, Rumpl, & Nordsieck (1977, hereafter MRN) and later elaborated by Draine & Lee (1984, hereafter DL), has been shown to be in good agreement with observations of interstellar extinction and absorption, polarization of starlight, and temperatures of graphite and silicates in the Milky Way. In this model, graphite is the carrier of the 2175 Å feature, and silicates are responsible for the 9.7 μm and 18 μm features. Although several other dust models have been advocated over the years, the advantage of the graphite-silicate model is that the optical efficiency factors for both grains of various sizes are readily available over a large range of wavelengths. In § 2, we assemble the basic data for the extinction curves and dust-to-gas ratios in the Milky Way, LMC, and SMC. In § 3, we fit the graphite-silicate model to the three empirical extinction curves and compute various optical and physical properties of interstellar dust for all three galaxies, including the extinction, absorption, and scattering optical depths as functions of wave-

lengths, the mass-density ratio of interstellar dust to neutral hydrogen, and the Kramers-Kronig relation of the interstellar medium as a whole. In § 4, we present a parameterized function for the three extinction curves over a large range of wavelengths and quantify some of the major differences among the three extinction curves. Discussion is given in § 5.

2. EMPIRICAL EXTINCTION PROPERTIES

We summarize in this section two observed properties of interstellar extinction in the Milky Way, LMC, and SMC. The first quantity we consider is the empirical extinction curve, defined here in a nondimensional form by

$$\xi(\lambda) \equiv A_\lambda / A_B \,, \tag{1}$$

where A_λ is the extinction in magnitudes at a wavelength λ and the subscript B refers to the blue photometric band. Since the results of interstellar extinction measurements have been most commonly analyzed using the color excess $E_{\lambda-V} \equiv A_\lambda - A_V$, divided by E_{B-V}, we write

$$\xi(\lambda) = [(E_{\lambda-V}/E_{B-V}) + R_V]/(1 + R_V) \,, \tag{2}$$

where $R_V \equiv A_V/E_{B-V}$ is the ratio of total-to-selective extinction and the subscript V refers to the visual photometric band. The second quantity we consider is a dimensionless dust-to-gas ratio

$$k \equiv 10^{21}(\tau_B/N_{\rm H\,I})\ {\rm cm}^{-2} \,, \tag{3}$$

where τ_B is the extinction optical depth in the B band and $N_{\rm H\,I}$ is the column density of neutral atomic hydrogen. Expressing the optical depth τ_B in terms of the color excess E_{B-V}, we have

$$k = 9.21 \times 10^{20}(1 + R_V)(E_{B-V}/N_{\rm H\,I})\ {\rm cm}^{-2} \,. \tag{4}$$

Throughout this section, the effective wavelengths of the B and V bands are taken to be $\lambda_B = 0.44$ μm and $\lambda_V = 0.55$ μm, respectively.

Virtually all determinations of the wavelength dependence of interstellar extinction have been so far limited to the Milky Way, LMC, and SMC. Beyond the Magellanic Clouds, our knowledge about the interstellar extinction curve fades quickly. Extinction, referred as the sum of absorption and scattering, is generally measured toward a pair of reddened and unreddened stars with nearly identical spectra. In the Milky Way, the O or B main-sequence stars are often chosen for comparison, partly because they have distinctive spectra and thus can be identified with high precision from their spectral lines, and partly because they are highly luminous and thus can be seen to large distances within our Galaxy. For the LMC and SMC at distances of about 55 and 65 kpc, respectively, the O and B stars are very difficult to observe. Instead, the OB supergiants, which are the brightest stars in the ultraviolet spectral region, are used to form the pair of reddened and unreddened stars. For any particular star, the observed values of $E_{\lambda-V}$ and E_{B-V} will be proportional to the number of dust grains along the line of sight, which varies from star to star. To form the average extinction curve from measurements along different lines of sight, it is common practice to normalize $E_{\lambda-V}$ with respect to E_{B-V}. Over the past years, numerous studies of the interstellar extinction curve have been carried out for the Milky Way, LMC, and SMC (see Massa & Savage 1989 and Fitzpatrick 1989 for a review). We summarize in Table 1 the most commonly used results of $E_{\lambda-V}/E_{B-V}$ at wavelengths 0.1 μm $\lesssim \lambda \lesssim$ 5 μm in the three galaxies.

TABLE 1

EMPIRICAL EXTINCTION CURVES

λ^{-1} (μm^{-1})	$E_{\lambda-V}/E_{B-V}$ (Milky Way)	λ^{-1} (μm^{-1})	$E_{\lambda-V}/E_{B-V}$ (LMC)	λ^{-1} (μm^{-1})	$E_{\lambda-V}/E_{B-V}$ (SMC)
0.21.....	−3.02	0.45	−2.92	0.45	−2.61
0.29.....	−2.91	0.61	−2.59	0.61	−2.47
0.45.....	−2.76	0.80	−2.22	0.80	−2.12
0.61.....	−2.58	1.82	0.00	1.82	0.00
0.80.....	−2.23	2.27	1.00	2.27	1.00
1.11.....	−1.60	2.70	1.70	2.70	1.67
1.43.....	−0.78	2.90	2.06	3.22	2.29
1.82.....	0.00	3.23	2.66	3.34	2.65
2.27.....	1.00	3.33	2.78	3.46	3.00
2.50.....	1.30	3.45	2.94	3.60	3.15
2.91.....	1.80	3.57	3.21	3.75	3.49
3.65.....	3.10	3.70	3.44	3.92	3.91
4.00.....	4.19	3.85	3.82	4.09	4.24
4.17.....	4.90	4.00	4.08	4.28	4.53
4.35.....	5.77	4.17	4.53	4.50	5.30
4.57.....	6.57	4.35	5.20	4.73	5.85
4.76.....	6.23	4.44	5.65	5.00	6.38
5.00.....	5.52	4.55	5.95	5.24	6.76
5.26.....	4.90	4.65	6.05	5.38	6.90
5.56.....	4.65	4.76	5.98	5.52	7.17
5.88.....	4.60	5.00	5.95	5.70	7.71
6.25.....	4.73	5.26	5.94	5.88	8.01
6.71.....	4.99	5.56	6.19	6.07	8.49
7.18.....	5.36	5.88	6.56	6.27	9.06
7.60.....	5.91	6.25	7.07	6.48	9.28
8.00.....	6.55	6.67	7.77	6.72	9.84
8.50.....	7.45	7.14	8.55	6.98	10.80
9.00.....	8.45	7.41	9.00	7.23	11.51
9.50.....	9.80	7.69	9.63	7.52	12.52
10.00.....	11.30	8.00	10.33	7.84	13.54

NOTES.—Entries at $\lambda^{-1} < 1$ μm^{-1} were taken as weighted averages from Koornneef (1983) and Rieke & Lebofsky (1985) for the Milky Way, Koornneef (1982) and Morgan & Nandy (1982) for the LMC, and Nandy, Morgan, & Houziaux (1984) and Bouchet et al. (1985) for the SMC. The rest of the entries were from Savage & Mathis (1979) for the Milky Way, Nandy et al. (1981) and Koornneef & Code (1981) for the LMC, and Prévot et al. (1984) for the SMC. A few Galactic entries near $\lambda^{-1} = 6.25$ μm were replaced by those given by Seaton (1979), since the Savage & Mathis (1979) curve at these entries contain a spurious artifact resulting from a luminosity mismatch (Massa & Savage 1989).

The use of equations (2) and (4) for each galaxy requires a mean value of R_V. Since the extinction curves in Table 1 were compiled from different sets of data, we derive the mean values of R_V appropriate for the three adopted curves for self-consistency. Most of the determinations of R_V are based on extrapolations of the near-infrared extinction measurements to infinite wavelength. This is because, on physical grounds, one can assume that $\xi(\lambda) \to 0$ as $\lambda \to \infty$, implying $R_V = -E_{\infty-V}/E_{B-V}$ from equation (2). The extrapolation method, though indirect, gives more accurate values of R_V than other methods that attempt to measure A_V directly (Aannestad & Purcell 1973), with the accuracy depending on the assumed form of $\xi(\lambda)$ at large wavelengths. We fit the simple function

$$\frac{E_{\lambda-V}}{E_{B-V}} = a_0 \frac{1 + R_V}{1 + (\lambda/\lambda_B)^2} - R_V \quad \text{for} \quad \lambda \gtrsim \lambda_V \,, \tag{5}$$

to the data listed in Table 1 at wavelengths longward of the V band. The results are shown as the solid curves in Figure 1, and the minimum χ^2 values of R_V and a_0 are listed in Table 2. We estimate that the standard deviations of the observed data about the best fits are 0.03, 0.06, and 0.04, respectively, for the Milky Way, LMC, and SMC, and the corresponding errors in both R_V and a_0 are roughly 0.02, 0.05, and 0.03, respectively,

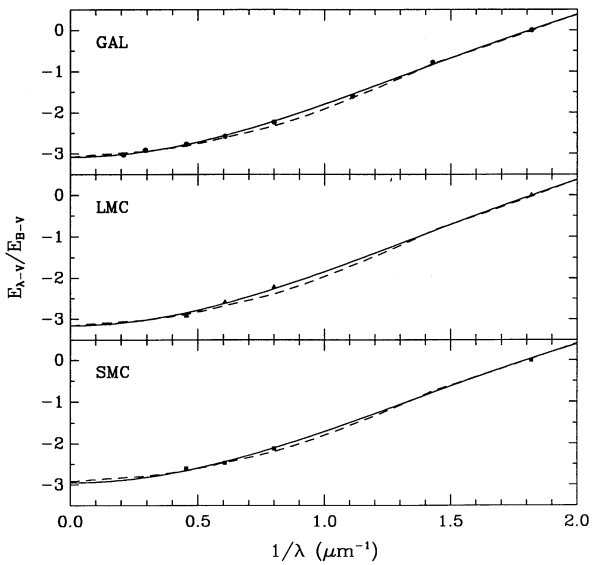

FIG. 1.—Near-infrared extinction curves for the Milky Way, LMC, and SMC. The data points were from Table 1. The solid curves represent our model in eq. (5) used to determine the values of R_V, while for comparison the dashed curves represent the classic van de Hulst curve no. 15 (van de Hulst 1949).

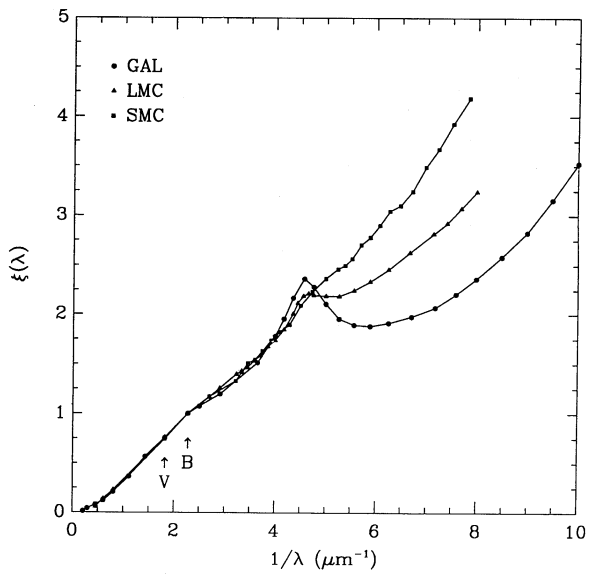

FIG. 2.—Empirical extinction curves for the Milky Way, LMC, and SMC. The data points are from Table 1 and references therein. The three curves form a sequence with decreasing strength of the 2175 Å feature and increasing level of the far-ultraviolet extinction.

for the Milky Way, LMC, and SMC. Evidently, our model in equation (5) provides excellent fits to the long-wavelength data in all three galaxies. In comparison, our formula closely resembles the classic van de Hulst curve no. 15 (van de Hulst 1949), shown as the dashed curves with the same values of R_V. Our estimates of R_V for the Milky Way, LMC, and SMC are also consistent with those derived by other authors using the van de Hulst curve no. 15 (Koornneef 1982, 1983; Rieke & Lebofsky 1985; Morgan & Nandy 1982; Nandy, Morgan, & Houziaux 1984; Bouchet et al. 1985).

Figure 2 shows the "mean" extinction curves for the Milky Way, LMC, and SMC. Here, we have plotted $\xi(\lambda)$ against $1/\lambda$ in μm^{-1}, computed from equation (2) with the values of $E_{\lambda-V}/E_{B-V}$ from Table 1 and the corresponding values of R_V from Table 2. The three mean extinction curves are similar at the infrared and visual bands, but, as already emphasized, differ substantially in the ultraviolet wavelengths. The far-ultraviolet extinction is smallest for the Milky Way but largest for the SMC, with the LMC in the middle. The most remarkable feature in the Galactic extinction curve is the broad bump centered near 2175 Å, with an average width (FWHM) of about 490 Å. Such a bump is also present in the LMC extinction curve with similar position and width but only about 1/2 in strength, while it is nearly absent in the SMC extinction curve with an upper limit of 1/9 or less in strength (see § 4 below). There is some evidence that the mean LMC extinction curve adopted here might not be representative of the LMC as a whole because it pertains to the 30 Dor region in the LMC (Clayton & Martin 1985; Fitzpatrick 1986). The interpretation of the mean SMC extinction curve as typical of the SMC might also be viewed with caution, since it was derived from only a few stars. Nevertheless, the Galactic, LMC, and SMC extinction curves shown in Figure 2 should be suitable for studies of dust at high redshifts because they span a wide range of possibilities and form a sequence with diminishing strength of the 2175 Å feature and increasing level of the far-ultraviolet extinction.

TABLE 2

INTERSTELLAR DUST PARAMETERS

Parameter	Milky Way	LMC	SMC
R_V	3.08	3.16	2.93
a_0	1.94	1.95	1.91
k	0.78	0.16	0.08
σ_s[a]	0.19	0.11	0.18
r_C	0.039	0.018	0.000
r_S	0.041	0.083	0.120
l	0.013	0.018	0.023
K	4.70	5.50	6.25

[a] Logarithmic dispersion in the dust-to-gas ratio along individual lines of sight within each galaxy, defined as $\sigma_s(\log k) \equiv \langle(\log k - \overline{\log k})^2\rangle^{1/2}$.

We now consider the empirical dust-to-gas ratios in the Milky Way, LMC, and SMC. The association of dust and gas in the Milky Way is clearly shown by a relatively close correlation between the color excess and the column density of either neutral atomic hydrogen or total neutral hydrogen in both atoms and molecules (Bohlin, Savage, & Drake 1978). Although the correlation with total neutral hydrogen is slightly better than the correlation with neutral atomic hydrogen, substantial scatters are present in both correlations. We will confine our discussion to neutral atomic hydrogen alone in order to make comparison with the LMC and SMC, because (1) the H I column density can be easily determined from the measurement of Lyα absorption profile, and (2) there has been little information about molecular hydrogen on scales of individual clouds in the LMC and SMC. Figure 3 shows the correlations between the color excess E_{B-V} and the H I column density N_H for all three galaxies. The data points were taken from Bohlin et al. (1978) for the Milky Way, Fitzpatrick (1985) for the LMC (30 Dor region), and Bouchet et al. (1985) for the

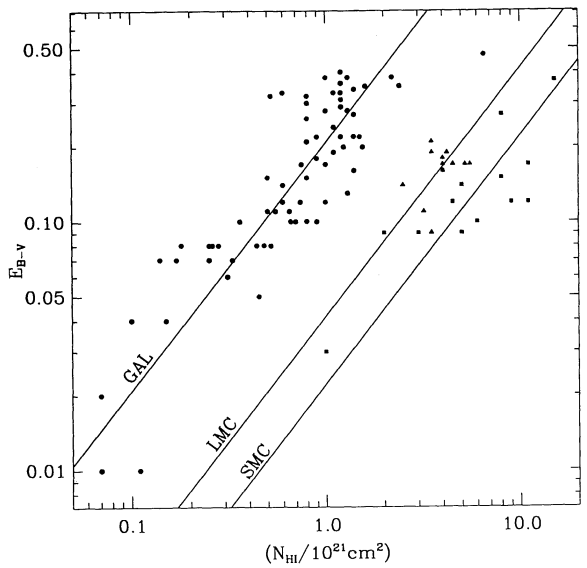

FIG. 3.—Correlations between the color excess of interstellar dust and the column density of neutral hydrogen for the Milky Way, LMC, and SMC. The data points were taken from Bohlin et al. (1978) for the Milky Way, Fitzpatrick (1985) for the LMC, and Bouchet et al. (1985) for the SMC. The lines represent the average ratios of the color excess to the column density derived by these authors.

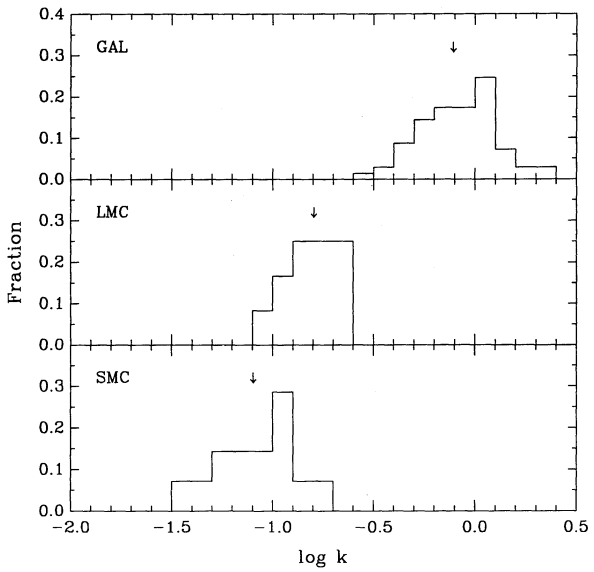

FIG. 4.—Distributions of the dust-to-gas ratio along individual lines of sight within the Milky Way, LMC, and SMC. The three histograms were derived using the data shown in Fig. 3, with the downward arrow indicating the mean dust-to-gas ratio in each galaxy.

SMC. The straight lines represent the best fits of the ratio $E_{B-V}/N_{\rm H\,I}$ derived by these authors. Although there is some scatter of the points about the mean in each galaxy, the three mean ratios of $E_{B-V}/N_{\rm H\,I}$ are significantly different. From equation (4), we have computed the corresponding values of k, with the results listed in Table 2. The three mean dust-to-gas ratios from the Milky Way to the LMC to the SMC form a decreasing sequence, in rough proportion of 1:1/5:1/10. Empirically, this appears to be correlated with the decreasing trend of the heavy-element abundances (1:1/3:1/8) from the Milky Way to the LMC to the SMC (Lequeux et al. 1979). Thus, the dust-to-metals ratio is roughly constant in these galaxies (to within 50% or so).

Finally, we are interested in some measure of the variation in the dust-to-gas ratio along individual lines of sight within the Milky Way, LMC, and SMC. This internal variation, together with the external variation in the mean dust-to-gas ratio from one galaxy to another, is relevant to studies of dust at high redshifts using quasars as probes. Since quasars are point sources, their lines of sight will pass through different locations for different galaxies. As a result, the total variance in the dust-to-gas ratio expected along random lines of sight passing through galaxies is the sum of the external variance from one galaxy to another and the internal variance within each galaxy. Using the three mean values of k, we have made a rough estimate for the external dispersion in the logarithm of the dust-to-gas ratio: $\sigma_g(\log k) \approx 0.4$. This estimate is quite uncertain because only three galaxies were used.[1] To estimate the internal dispersion, we plot in Figure 4 the distributions of the dust-to-gas ratio along individual lines of sight within the Milky Way, LMC, and SMC. The three histograms, though differing substantially in the means, have a similar logarithmic dispersion in the dust-to-gas ratio. The estimates of the internal dispersion, listed in Table 2, lie in the range $0.1 \lesssim \sigma_s(\log k) \lesssim 0.2$ for the three galaxies. The internal dispersions appear to be smaller than the external dispersion. We conclude that the variation in the dust-to-gas along random lines of sight passing through galaxies is probably dominated by the variation from one galaxy to another, rather than the variation within each galaxy.

[1] In a sample of 58 spiral galaxies, Devereux & Young (1990) found the logarithmic dispersion of about 0.5 in the mass ratio of warm dust to neutral hydrogen. If the fraction of warm to total dust is roughly the same in all the spirals, this large sample of galaxies indicates $\sigma_g(\log k) \approx 0.5$ for the external dispersion from galaxy to galaxy.

3. INTERSTELLAR GRAIN PROPERTIES

We compute in this section some optical and physical properties of interstellar dust grains in the Milky Way, LMC, and SMC. In particular, we are interested in the extinction, absorption, and scattering optical depths, the mass ratio of interstellar dust to neutral hydrogen, and the Kramers-Kronig relation. Our calculations are based on the MRN–DL interstellar dust models with the graphite and silicate abundances optimized from fits to the three empirical extinction curves. We begin by defining $N_X(a)da$ as the column density of dust grains of type X with radii between a and $a + da$. The extinction, absorption, or scattering optical depth as a function of wavelength is then given by

$$\tau(\lambda) = \sum_X \int_{a_{\rm min}}^{a_{\rm max}} da\, \pi a^2 N_X(a) Q_X(\lambda, a)\,, \qquad (6)$$

where $Q_X(\lambda, a)$ is the corresponding efficiency factor of grains of type X at wavelength λ and radius a, $a_{\rm max}$ and $a_{\rm min}$ are, respectively, the upper and lower size cutoffs, and the sum is over all components of the grains under consideration. By definition, the three optical depths are simply related by

$$\tau_{\rm ext}(\lambda) = \tau_{\rm abs}(\lambda) + \tau_{\rm sca}(\lambda)\,. \qquad (7)$$

We first consider the extinction optical depth in order to determine the various parameters in equation (6). The interstellar extinction curve, as defined in the previous section, can now be written as

$$\xi(\lambda) = \tau_{\rm ext}(\lambda)/\tau_B \,, \tag{8}$$

where again τ_B is the extinction optical depth in the B band.

The composition and size distribution of interstellar grains have often been inferred from the observed extinction curve. When equation (8) is compared with the extinction data in the Milky Way, it is found that no model for grains of a single composition and size can fit the data. The composition can also be directly identified through spectral features in both absorption and emission of interstellar dust, but the size distribution is almost entirely inferred from modeling the extinction data. Carbon, in the form of graphite or in an amorphous state, has been identified via the broad interstellar absorption band centered near 2175 Å, and silicates have been identified via the 9.7 μm and 18 μm features in both emission and absorption of interstellar dust (see Stein & Soifer 1983 for a review). Most of the carbon may be produced in carbon stars (C > O), while most of the silicates are probably from stars with normal abundances (C < O). Although several other materials have been identified, graphite and silicates are believed to be two major constituents of interstellar dust. An extensive modeling of the Galactic extinction curve using a mixture of pure graphite and silicate grains has been first accomplished by MRN and later improved by DL. This model has also shown to be consistent with interstellar absorption, polarization of starlight, and temperatures of graphite and silicates (Mathis 1979; Mathis & Wallenhorst 1981; DL), although it may require some modification to account for new emission data (Puget & Léger 1989). Since our goal is to provide a wide range of possibilities in the interstellar grain properties that are self-consistent with the three empirical extinction curves, only graphite and silicate grains are considered in our calculations.

We adopt the MRN–DL graphite-silicate dust model in which the size distribution $N_X(a)$ was taken from MRN and the efficiency factors $Q_X(\lambda, a)$ were taken from DL. Both graphite and silicate grains are assumed to be spherical and uncoated. In an extensive fitting of the Galactic extinction curve, MRN found that the size distribution for both graphite and silicates can be well approximated by a simple power-law form, $N_X(a) \propto a^{-\beta}$, with the power index, $\beta \approx 3.5$, and the lower and upper size cutoffs, $a_{\rm min} \approx 0.005$ μm and $a_{\rm max} \approx 0.25$ μm. The values of these parameters, originally determined over a small range of wavelengths, have later been found to predict adequately the Galactic extinction curve over a much larger range of wavelengths: 0.1 μm $\lesssim \lambda \lesssim$ 100 μm (DL). These values are adopted in our calculations, because we find that there is no need to adjust them in fitting all three extinction curves. In an important paper, DL derived the best sets of the extinction, absorption, and scattering efficiency factors for spherical graphite and silicate grains. The imaginary parts of the dielectric functions were heavily guided from available laboratory measurements and astronomical observations, while the real parts were based on the appropriate Kramers-Kronig dispersion relations. Their results of $Q_X(\lambda, a)$, as tabulated by Draine (1987), cover wavelengths 304 Å $\le \lambda \le$ 2000 μm and radii 0.005 μm $\le a \le$ 1 μm.

To establish our notation, we write the MRN size distribution in the form

$$N_X(a)da = N_X(a/a_V)^{-\beta} d(a/a_V) \quad \text{for} \quad a_{\rm min} \le a \le a_{\rm max} \,, \tag{9}$$

where the subscript X denotes either graphite (C) or silicates (S) and a_V is an arbitrary radius. We choose a_V such that

$$a_V^3 \equiv N_X^{-1} \int_{a_{\rm min}}^{a_{\rm max}} da\, N_X(a) a^3 \,. \tag{10}$$

In this way, the constant of proportionality N_X becomes the volume-weighted column density of grains of type X. Integrating equation (10), we have $a_V \approx 0.737$ μm for the adopted parameters $\beta = 3.5$, $a_{\rm min} = 0.005$ μm, and $a_{\rm max} = 0.25$ μm. Substituting equations (9) and (6) into equation (8) then gives

$$\xi(\lambda) = \sum_X r_X \int_{a_{\rm min}}^{a_{\rm max}} d(a/a_V)(a/a_V)^{2-\beta} Q_X^{\rm ext}(\lambda, a) \,, \tag{11}$$

with

$$r_X \equiv \frac{\pi a_V^2 N_X}{\tau_B} = \frac{1/71 \times 10^{13}}{k} \left(\frac{N_X}{N_{\rm H\,I}}\right), \tag{12}$$

where $Q_X^{\rm ext}$ is the extinction efficiency factor of grains of type X, and the sum is over the two components of graphite and silicates. We fit the model to empirical extinction curves in the form of $\xi(\lambda)$ to determine the constants r_X that control the relative abundances of graphite and silicates to neutral hydrogen. Since the empirical extention curve does not depend on the dust-to-gas ratio, the inferred values of r_X are independent of k.

Figure 5 shows the comparisons between the model and empirical extinction curves in the Milky Way, LMC, and SMC. The short and long-dashed curves represent, respectively, the relative contributions from graphite and silicate grains, with the sum of the two shown by the solid curves. The minimum χ^2 values of r_X for graphite and silicates are given in Table 2 for the three galaxies. We estimate that the standard deviations of the observed data about the best fits are 0.06, 0.06, and 0.13, respectively, for the Milky Way, LMC, and SMC, and the corresponding errors in r_X are roughly 0.002, 0.002, and 0.003, respectively, for the Milky Way, LMC, and

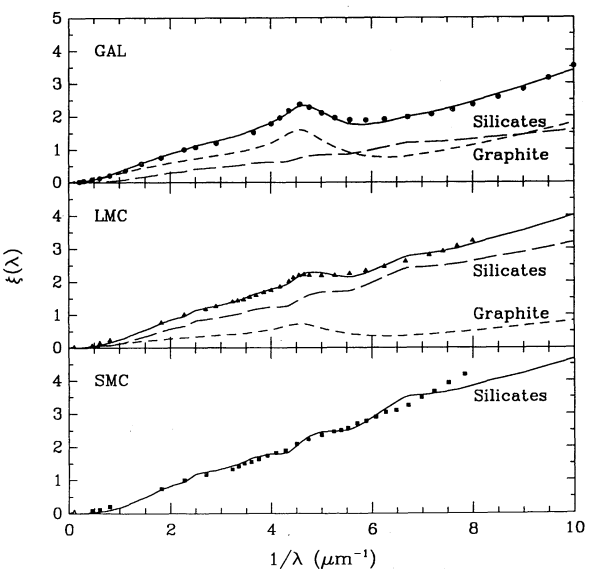

FIG. 5.—Comparisons between the model and empirical extinction curves in the Milky Way, LMC, and SMC. The short and long-dashed lines show, respectively, the relative contributions from graphite and silicate grains, with the sum of the two shown as the solid lines.

SMC. The three model extinction curves, derived by varying only the relative abundances of graphite and silicates, agree very well with the empirical extinction curves, although some minor differences exist. We have checked that these minor differences cannot be eliminated by including β, $a_{\min}$, and $a_{\max}$ as additional free parameters. It is remarkable that the values of these parameters are roughly optimized for all three galaxies. As DL have pointed out, one should not expect detailed agreement between the model and empirical extinction curves, because of the uncertainties involved in the efficiency factors. Thus, the graphite-silicate model appears to be compatible with the extinction data in all three galaxies. The graphite component is necessary in providing the broad excess extinction centered near 2175 Å, while the silicate component is essential in reproducing the 9.7 μm and 18 μm features in the Milky Way (DL). We find that the Galactic and LMC extinction curves require a mixture of both graphite and silicate grains with the abundance ratio of $r_C/r_S = 0.95$ and 0.22, respectively, but the SMC extinction curve can be fitted by silicate grains alone. For the Milky Way, our estimate of $r_C/r_S = 0.95$ is slightly larger than the values of 0.93 and 0.89 derived by MRN and DL. Our results for the three galaxies suggest that the abundance ratio of graphite to silicates diminishes from the Milky Way to the LMC to the SMC.

We can now calculate various predictions from the graphite-silicate models for the Milky Way, LMC, and SMC. For the absorption optical depth, we define, by analogy with equation (8), a dimensionless absorption curve

$$\eta(\lambda) \equiv \tau_{\rm abs}(\lambda)/\tau_B = \sum_X r_X \int_{a_{\min}}^{a_{\max}} d(a/a_V)(a/a_V)^{2-\beta} Q_X^{\rm abs}(\lambda, a) , \quad (13)$$

while for the scattering optical depth, we consider the wavelength dependence of the albedo

$$\omega(\lambda) \equiv \tau_{\rm sca}(\lambda)/\tau_{\rm ext}(\lambda) = \xi^{-1}(\lambda) \sum_X r_X \int_{a_{\min}}^{a_{\max}} d(a/a_V)(a/a_V)^{2-\beta} Q_X^{\rm sca}(\lambda, a) . \quad (14)$$

Here $Q_X^{\rm abs}$ and $Q_X^{\rm sca}$ are, respectively, the absorption and scattering efficiency factors of grains of type X. Using the values of r_X derived above, we have computed the absorption and albedo curves from equations (13) and (14). The results are shown in Figure 6 for the three galaxies. It can be seen from the upper panel that the 2175 Å absorption feature is the strongest in the Milky Way but weak or absent in the LMC and SMC. The crossing of the three absorption curves at $\lambda \approx 0.18$ μm is the result of the normalization chosen in equation (13). The three albedo curves shown in the lower panel differ substantially in the range 0.2 μm $\lesssim \lambda \lesssim$ 1 μm and approach asymptotically 0.4–0.5 at extreme ultraviolet wavelengths. For the Milky Way, the albedo curve we derived here is similar to that derived by DL. Since the absorption and extinction approach each other at large wavelengths, we choose to tabulate the three albedo curves rather than the absorption curves. The results of $\omega(\lambda)$ over the range of wavelengths 300 Å $\lesssim \lambda \lesssim$ 2000 μm are listed in Table 3 for the three galaxies.

The mass-density ratio of interstellar dust to neutral hydrogen is simply proportional to the observed dust-to-gas ratio. The constant of proportionality depends on the optical and physical properties of interstellar grains and can be estimated from the graphite-silicate models derived above. We define a dimensionless constant l by the relation

$$\rho_D/\rho_{\rm H\,I} \equiv kl , \quad (15)$$

TABLE 3

PREDICTED ALBEDO CURVES

λ (μm)	log ω (Milky Way)	log ω (LMC)	log ω (SMC)	λ (Å)	log ω Milky Way	log ω (LMC)	log ω (SMC)
2000	−7.77	−7.81	−7.84	4000	−0.25	−0.14	−0.06
1000	−7.16	−7.21	−7.24	3700	−0.25	−0.14	−0.06
500	−6.55	−6.60	−6.64	3440	−0.25	−0.14	−0.06
200	−5.76	−5.81	−5.85	3000	−0.25	−0.14	−0.07
100	−5.17	−5.22	−5.26	2740	−0.25	−0.14	−0.07
50.0	−4.60	−4.66	−4.70	2500	−0.26	−0.15	−0.07
30.0	−4.11	−4.22	−4.28	2400	−0.27	−0.15	−0.06
25.0	−3.92	−4.07	−4.15	2300	−0.30	−0.17	−0.07
21.0	−3.74	−3.94	−4.04	2175	−0.33	−0.18	−0.08
18.0	−3.61	−3.87	−4.01	2100	−0.33	−0.19	−0.09
16.0	−3.37	−3.67	−3.86	2000	−0.32	−0.19	−0.11
14.0	−3.02	−3.28	−3.44	1900	−0.31	−0.20	−0.14
13.0	−2.97	−3.21	−3.35	1800	−0.32	−0.23	−0.19
12.0	−2.96	−3.20	−3.32	1700	−0.34	−0.27	−0.24
11.0	−2.95	−3.20	−3.32	1600	−0.36	−0.31	−0.29
9.70	−2.94	−3.23	−3.38	1500	−0.38	−0.36	−0.35
8.50	−2.62	−3.08	−3.54	1400	−0.39	−0.41	−0.42
8.00	−2.30	−2.77	−3.55	1300	−0.37	−0.40	−0.41
7.00	−1.84	−2.06	−2.41	1216	−0.38	−0.41	−0.42
4.80	−1.34	−1.40	−1.50	1100	−0.39	−0.42	−0.44
3.40	−1.00	−1.00	−1.00	1000	−0.42	−0.44	−0.46
2.20	−0.63	−0.59	−0.49	912	−0.45	−0.46	−0.48
1.65	−0.47	−0.40	−0.28	800	−0.44	−0.46	−0.48
1.25	−0.36	−0.28	−0.16	700	−0.43	−0.45	−0.47
0.90	−0.29	−0.20	−0.10	600	−0.40	−0.44	−0.45
0.70	−0.26	−0.16	−0.07	504	−0.35	−0.39	−0.42
0.55	−0.26	−0.15	−0.06	400	−0.35	−0.39	−0.41
0.44	−0.26	−0.14	−0.06	304	−0.33	−0.36	−0.38

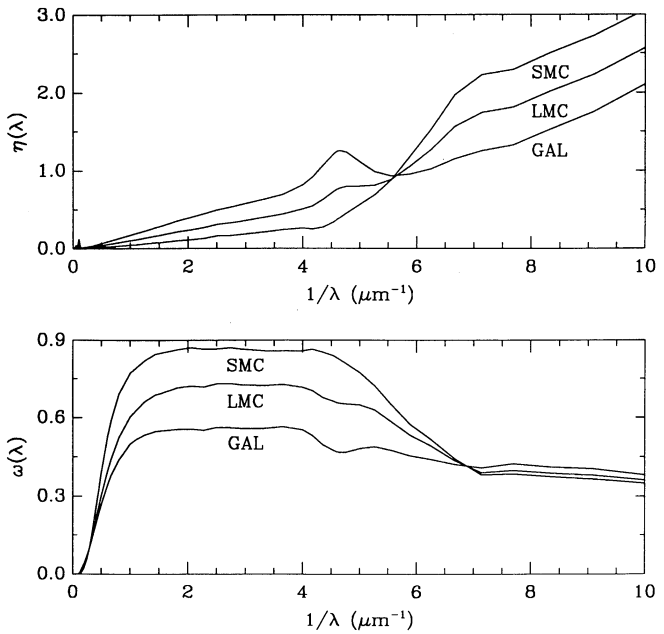

FIG. 6.—Predicted absorption and albedo curves for the graphite-silicate mixtures in the Milky Way, LMC, and SMC. The upper panel shows the absorption curves computed from eq. (13), while the lower panel shows the albedo curves computed from eq. (14).

where ρ_D and $\rho_{\rm H\,I}$ are, respectively, the mass densities of dust and neutral hydrogen, and again k is the empirical dust-to-gas ratio. One can easily show that

$$\frac{\rho_D}{\rho_{\rm H\,I}} = \frac{4\pi}{3m_{\rm H}N_{\rm H\,I}} \sum_X \rho_X \int_{a_{\rm min}}^{a_{\rm max}} da\, a^3 N_X(a)\,, \qquad (16)$$

where ρ_X is the grain density of type X and other symbols have their usual meanings. Equation (16) pertains only to the graphite and silicate grains. Combining equations (9), (15), and (16), we obtain

$$l = 0.059 \sum_X r_X(\rho_X/g\ {\rm cm}^{-3})\,. \qquad (17)$$

To estimate the constant l, we adopt $\rho_C = 2.26$ g cm^{-3} for graphite and $\rho_S = 3.3$ g cm^{-3} for silicates (DL). The values of l are given in Table 2 for the Milky Way, LMC, and SMC. We find, together with the dust-to-gas ratios, that the mass-density ratios of interstellar dust to neutral hydrogen are in rough proportion of 1:1/3:1/5 from the Milky Way to the LMC to the SMC.

The Kramers-Kronig relation can be applied to the interstellar medium as a whole. In this case, it relates the integral of the extinction optical depth over all wavelengths to the volume occupied by dust grains and can be used to constrain the total amount of interstellar dust from the extinction curve (Purcell 1969). Here, we compute the Kramers-Kronig integral relations in the Milky Way, LMC, and SMC from the graphite and silicate models. We define a dimensionless integral over the extinction curve

$$K \equiv \frac{1}{\lambda_B}\int_0^\infty d\lambda\, \xi(\lambda)\,. \qquad (18)$$

Following the derivation by Purcell (1969), we have

$$K = \frac{4\pi^3}{\lambda_B \tau_B}\sum_X F_X \int_{a_{\rm min}}^{a_{\rm max}} da\, a^3 N_X(a) = \frac{4\pi^2 a_V}{\lambda_B}\sum_X F_X r_X\,, \qquad (19)$$

where F_X is a constant depending on the dielectric constant in the low-frequency limit and shape of grains of type X. For spherical particles, F_X is independent of the shape and approaches unity for conducting grains, i.e., with infinite dielectric constant (Purcell 1969). Taking $F_C = 0.996$ for graphite and $F_S = 0.786$ for silicates (DL), we compute the values of K from equation (19) and list the results in Table 2 for the three galaxies. In comparison, we also compute the values of K from equation (18) by integrating the three extinction curves over the observed range of wavelengths. We find that the observed data contribute only 35%–55% to the Kramers-Kronig integral, while the far-infrared extinction, even though small, is responsible for most of the missing contributions. A finite integral requires that $\xi(\lambda)$ must approach zero faster than $1/\lambda$ in the limit $\lambda \to \infty$.

4. FITTING FUNCTION FOR THE EXTINCTION CURVES

We present in this section an analytic representation for the three extinction curves in the Milky Way, LMC, and SMC. Several fitting functions for the Galactic extinction curve have been proposed in the past. Most of them are applicable only to the ultraviolet part of the extinction curve (Savage 1975; Seaton 1979; Fitzpatrick & Massa 1990), while those extending to the near-infrared part involve high-order polynomials that must be joined in various regions of wavelengths (Cardelli, Clayton, & Mathis 1989). Here, we introduce a fitting function that is valid not only over the observed range of wavelengths but also over the full range as predicted by the graphite-silicate models and suitable for all three extinction curves. We emphasize, however, that any parameterized expressions are not unique and thus of limited physical significance; they are merely continuous representations of extinction data. For this reason, our formula is used to represent the Galactic, LMC, and SMC extinction curves over a large range of wavelengths. It is also used to quantify some major differences among the three extinction curves, including the strengths of the 2175 Å, 9.7 μm, and 18 μm features and the shapes of the far-ultraviolet and far-infrared extinction. One advantage of our formula is that it approaches zero faster than $1/\lambda$ at infinite wavelengths and hence gives a finite integral for the Kramers-Kronig relation of the interstellar medium.

Our fitting function covering all wavelengths consists of six terms of the form

$$\xi(\lambda) = \sum_{i=1}^{6} \frac{a_i}{(\lambda/\lambda_i)^{n_i} + (\lambda_i/\lambda)^{n_i} + b_i}\,, \qquad (20)$$

where a_i, λ_i, b_i, n_i are "free" parameters. All six terms are positive: three of them represent the "background" (BKG), far-ultraviolet (FUV), and far-infrared (FIR) extinctions, while the other three represent the 2175 Å, 9.7 μm, and 18 μm extinction features. The parameter n_i is introduced only for the FUV term and has been set to $n_i = 2$ for all the other terms. The contribution of each term ($n_i \geq 2$) to the Kramers-Kronig relation can be calculated by the integral

$$K_i = \frac{1}{\lambda_B}\int_0^\infty d\lambda\, \frac{a_i}{(\lambda/\lambda_i)^{n_i} + (\lambda_i/\lambda)^{n_i} + b_i}\,. \qquad (21)$$

TABLE 4

ANALYTIC EXTINCTION CURVE PARAMETERS

Parameter	a_i	λ_i (μm)	b_i	n_i	K_i
Milky Way Galaxy					
BKG	165.	0.047	90.	2.0	2.89
FUV	14.	0.08	4.00	6.5	0.31
2175 Å	0.045	0.22	−1.95	2.0	0.16
9.7 μm	0.002	9.7	−1.95	2.0	0.31
18 μm	0.002	18.	−1.80	2.0	0.28
FIR	0.012	25.	0.00	2.0	0.76
Large Magellanic Cloud					
BKG	175.	0.046	90.	2.0	3.00
FUV	19.	0.08	5.50	4.5	0.56
2175 Å	0.023	0.22	−1.95	2.0	0.08
9.7 μm	0.005	9.7	−1.95	2.0	0.77
18 μm	0.006	18.	−1.80	2.0	0.86
FIR	0.020	25.	0.00	2.0	1.26
Small Magellanic Cloud					
BKG	185.	0.042	90.	2.0	2.89
FUV	27.	0.08	5.50	4.0	0.91
2175 Å	0.005	0.22	−1.95	2.0	0.02
9.7 μm	0.010	9.7	−1.95	2.0	1.55
18 μm	0.012	18.	−1.80	2.0	1.72
FIR	0.030	25.	0.00	2.0	1.89

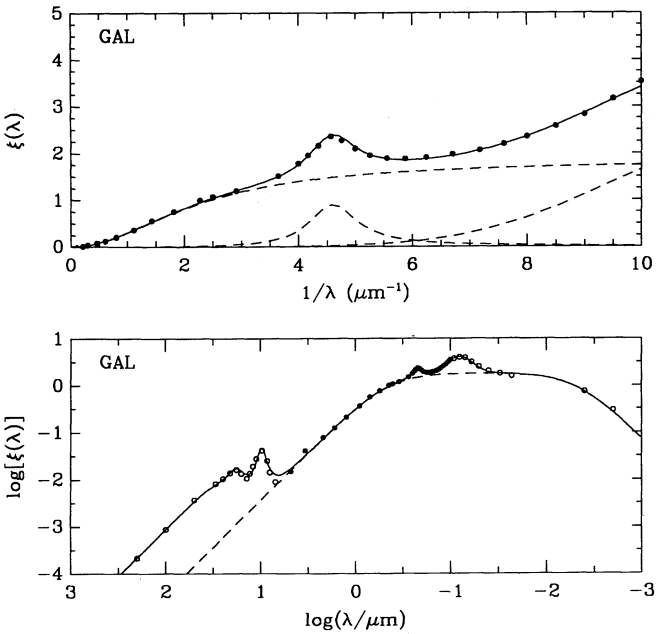

FIG. 7.—Extinction curve for the Milky Way. The filled circles are the data points, while the open circles are the model predictions. The solid curve in the upper or lower panel represents an analytic fit from eq. (20). The three dashed curves in the upper panel represent the 2175 Å feature, the far-ultraviolet extinction, and a background component, while the dashed curve in the lower panel indicates the background component over a large range of wavelengths.

We use the dimensionless constant K_i to indicate the relative strength of each term. Equation (20) has 19 free parameters to cover the full range of wavelengths from FIR to X-ray, while it may have 10 free parameters with three terms over the observed range of wavelengths between 0.1 μm and 5 μm. In comparison, the Seaton (1979) curve covering wavelengths 0.1 μm $\leq \lambda \leq$ 0.4 μm has 10 adopted parameters; the Fitzpatrick & Massa (1990) form covering similar wavelengths has six fitting parameters with three additional fixed numerical values; and the Cardelli et al. (1989) curve covering wavelengths 0.1 μm $\leq \lambda \leq 4$ μm requires more than 20 numerical values.

We have fitted equation (20) to the three extinction curves in the Milky Way, LMC, and SMC. The eye-fitted estimates of the parameters are summarized in Table 4, with the values of K_i computed from equation (21). The results of our fits are shown in Figures 7–9 for the three galaxies. The filled points in each of the figures are the observed data, while the open points are the graphite-silicate model predictions derived from the previous section and matched here for continuity with the data, and three of them at shortest wavelengths are the extensions of the graphite-silicate model from the ionizing-UV range to X-ray energies derived by Martin & Rouleau (1989). Although the open points should be subject to observational verifications, they represent plausible extensions of the three observed extinction curves to much shorter and longer wavelengths. Nevertheless, our fitting function provides excellent fits to all three extinction curves, not only over the observed range of wavelengths shown in the upper panels but also over the full range of wavelengths shown in the lower panels. The maximum difference between equation (20) and the observed extinction curve is $\Delta\xi \lesssim 0.1$ for all three galaxies. According to equation (20), the three extinction curves contain a very similar broad background component, shown as the dashed curve in each of the lower panels. This component dominates the extinction curve in the 0.5–5.0 μm region and can be reduced roughly to equation (5) used in § 2. It is possible that the background component we considered here represents the so-called universal near-infrared extinction curve as often approximated by $\xi(\lambda) \propto \lambda^{-\alpha}$ with $\alpha \approx 1.6$–1.8 (Mathis 1990 and references therein).

We use the fitting function presented above to quantify some major observed and predicted differences in the Galactic, LMC, and SMC extinction curves. Each of the five terms in equation (20) with $n_i = 2$ is equivalent to a "Drude" profile

$$D(\lambda; \lambda_i, \Gamma_i) = \frac{1}{[(\lambda/\lambda_i) - (\lambda_i/\lambda)]^2 + (\Gamma_i/\lambda_i)^2}, \qquad (22)$$

with the peak of the position at wavelength λ_i and the full width of the profile at half-maximum $\Gamma_i = \lambda_i(2 + b_i)^{1/2}$. The Drude profile has recently been adopted to fit the shape of the 2175 Å feature, because of its slightly better match to the data than a Lorentz profile (Fitzpatrick & Massa 1990). Since the Drude profile is the full solution for the absorption and scattering cross sections due to a forced, damped harmonic oscillator, its resemblance to extinction features may indicate that some optical properties of grains could be interpreted in terms of simple harmonic oscillators. Thus, the decomposition in our fitting function may have physical basis. In fact, the BKG FUV, and 2175 Å terms, shown as the dashed curves in each of the upper panels of Figures 7–9, roughly resemble the contributions of the big (BGs), very small (VSGs), and polycyclic aromatic hydrocarbon (PAHs) grains proposed by Désert, Boulanger, & Puget (1990) in their interstellar dust models. We find that the extinction curves from the Milky Way to the LMC to the SMC show the following observed or predicted sequences with decreasing strength of the 2175 Å feature and

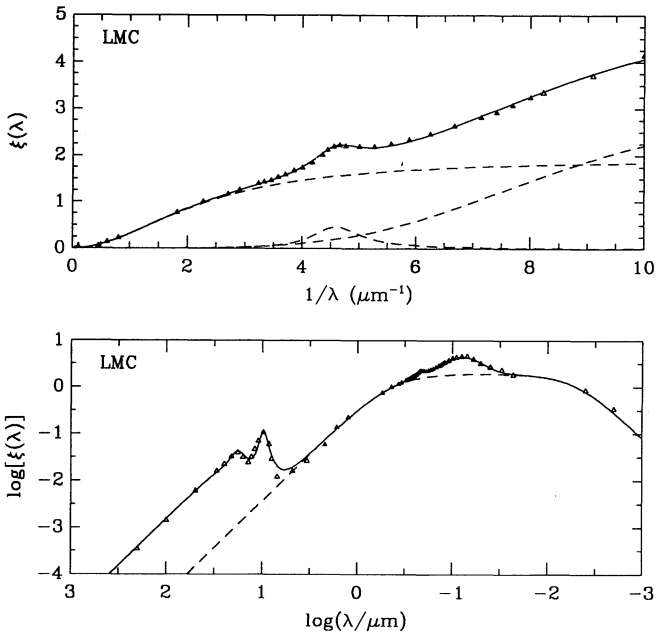

FIG. 8.—Extinction curve for the LMC. The filled triangles are the data points, while the open triangles are the model predictions. The solid curve in the upper or lower panel represents an analytic fit from eq. (20). The three dashed curves in the upper panel represent the 2175 Å feature, the far-ultraviolet extinction, and a background component, while the dashed curve in the lower panel indicates the background component over a large range of wavelengths.

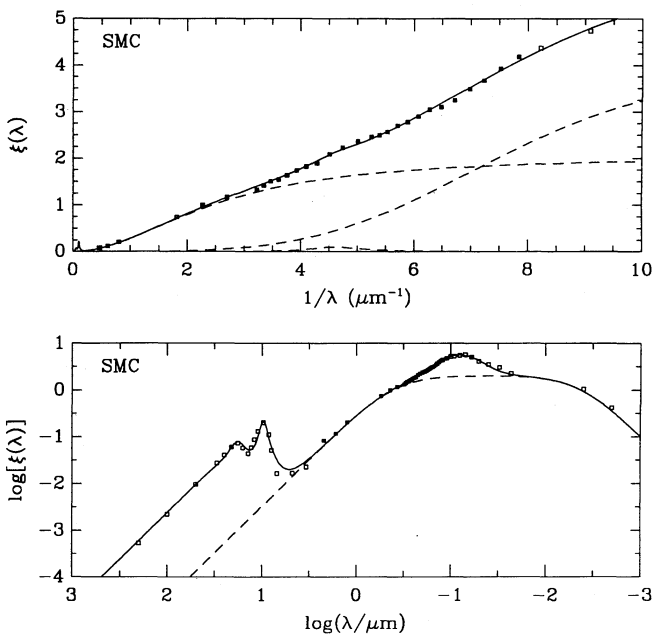

FIG. 9.—Extinction curve for the SMC. The filled squares are the data points, while the open squares are the model predictions. The solid curve in the upper or lower panel represents an analytic fit from eq. (20). The three dashed curves in the upper panel represent the 2175 Å feature, the far-ultraviolet extinction, and a background component, while the dashed curve in the lower panel indicates the background component over a large range of wavelengths.

increasing strengths of the 9.7 μm and 18 μm features and the FUV and FIR extinction. The proportions of these strengths in the three galaxies can be easily inferred from the values of K_i listed in Table 4. It is interesting to note that, if the predictions from the graphite-silicate models are correct, the most conspicuous "feature" in the extinction curve would be the very broad FUV bump centered near 800 Å rather than the 2175 Å bump.

5. DISCUSSION

Our main conclusion is that the standard graphite-silicate model appears to account well for the three observed extinction curves in the Milky Way, LMC, and SMC with only the adjustment of the graphite-to-silicate ratio. We find that the Galactic extinction curve requires roughly an equal amount of graphite and silicate grains, while the SMC extinction curve can be reproduced by silicate grains alone, with the LMC extinction curve representing an intermediate situation. From the graphite-silicate models, we have computed various optical and physical properties of interstellar dust in the three galaxies, including the absorption and scattering optical depths as functions of wavelength, the mass-density ratio of interstellar dust to neutral hydrogen, and the Kramers-Kronig relation of the interstellar medium. Another conclusion from our study is that the fitting function introduced here provides an excellent fit to the three extinction curves over the full range of wavelengths as either given by observations or predicted by the models. We have used this fitting function to quantify some major differences in the three extinction curves. In summary, the Milky Way, LMC, and SMC display the following observed or predicted proportions: (1) 1:1/5:1/10 in the dust-to-gas ratio; (2) 1:1/3:1/8 in the abundance of heavy elements; (3) 1:1/4:1/6 in the mass ratio of dust to neutral hydrogen; (4) 1:1/2:1/8 in the strength of the 2175 Å feature; (5) 1:2:5 in the strength of the 9.7 μm feature; (6) 1:3:6 in the strength of the 18 μm feature; (7) 1:2:3 in the FIR extinction; and (8) 1:2:3 in the FUV extinction.

Our results can be used as a tool for many studies of dust at high redshifts. They are useful and sometimes essential in determining the importance of dust on cosmological scales, such as the obscuration of quasars by intervening galaxies, the absorption of Lyα photons by internal dust in galaxies, the comoving mass density of dust in galaxies, the dust attenuation of ultraviolet background radiation, and the dust orgin of the cosmic submillimeter background (e.g., Heisler & Ostriker 1988; Draine & Shapiro 1989; Wright 1990; Charlot & Fall 1991; Fall & Pei 1992). In recent years, it has become possible to search for cosmologically distributed dust using quasars as probes. Nearly all of the searches in quasar absorption-line systems rely heavily on the strength of the 2175 Å feature and/or the slope of the FUV extinction in the assumed extinction curve. As a result, the inferred values of the dust-to-gas ratio depends on whether the extinction curve is assumed to be that in the Milky Way, LMC, or SMC. For this reason, all the quantities we derived here are based only on the shape of the extinction curves in the Milky Way, LMC, and SMC. They are independent of the dust-to-gas ratios in the three galaxies and can be applied to other galaxies if they contain Galactic or Magellanic-type dust. From the absence of the 2175 Å feature and low abundances of heavy elements and dust in damped Lyα systems, LMC and SMC-type dust may be favored observationally at high redshifts rather than Galactic-type dust (Pei et al. 1991 and references therein).

I would like to thank Bruce Draine, Mike Fall, Edward Fitzpatrick, and Ed Turner for useful conversations and suggestions and an anonymous referee for helpful comments. This work was supported in part by NASA grant NAGW-2448.

REFERENCES

Aannestad, P. A., & Purcell, E. M. 1973, ARA&A, 11, 309
Bohlin, R. C., Savage, B. D., & Drake, J. F. 1978, ApJ, 224, 291
Bouchet, P., Lequeux, J., Maurice, E., Prévot, L., & Prévot-Burnichon, M. L. 1985, A&A, 149, 330
Cardelli, J. A., Clayton, G. C., & Mathis, J. S. 1989, ApJ, 345, 245
Charlot, S., & Fall, S. M. 1991, ApJ, 471, 378
Clayton, G. C., & Martin, P. G. 1985, ApJ, 288, 558
Désert, F.-X., Boulanger, F., & Puget, J. L. 1990, A&A, 237, 215
Devereux, N. A., & Young, J. S. 1990, ApJ, 359, 42
Draine, B. T. 1987, preprint
Draine, B. T., & Lee, H. M. 1984, ApJ, 285, 89 (DL)
Draine, B. T., & Shapiro, P. R. 1989, ApJ, 344, L45
Fall, S. M., & Pei, Y. C. 1992, ApJ, submitted
Fitzpatrick, E. L. 1985, ApJ, 299, 219
———. 1986, AJ, 92, 1068
———. 1989, in IAU Symp. 135, Interstellar Dust, ed. L. J. Allamandola & A. G. G. M. Tielens (Dordrecht: Kkuwer), 37
Fitzpatrick, E. L., & Massa, D. 1990, ApJS, 72, 163
Heisler, J., & Ostriker, J. P. 1988, ApJ, 332, 543
Koornneef, J. 1982, A&A, 107, 247
———. 1983, A&A, 128, 84
Koornneef, J., & Code, A. D. 1981, ApJ, 247, 860
Lequeux, J., Peimbert, M., Rayo, J. F., Serrano, A., & Torres-Peimbert, S. 1979, A&A, 80, 155
Martin, P. G., & Rouleau, F. 1989, in Extreme Ultraviolet Astronomy, ed. R. F. Malina & S. Bowyer (Oxford: Pergamon), in press
Massa, D., & Savage, B. D. 1989, in IAU Symp. 135, Interstellar Dust, ed. L. J. Allamandola & A. G. G. M. Tielens (Dordrecht: Kluwer), 3
Mathis, J. S. 1979, ApJ, 232, 747
———. 1990, ARA&A, 28, 37
Mathis, J. S., Rumpl, W., & Nordsieck, K. H. 1977, ApJ, 217, 425 (MRN)
Mathis, J. S., & Wallenhorst, S. G. 1981, ApJ, 244, 483
Morgan, D. H., & Nandy, K. 1982, MNRAS, 199, 979
Nandy, K., Morgan, D. H., & Houziaux, L. 1984, MNRAS, 211, 895
Nandy, K., Morgan, D. H., Willis, A. J., Wilson, R., & Gondhalekar, P. M. 1981, MNRAS, 196, 955
Pei, Y. C., Fall, S. M., & Bechtold, J. 1991, ApJ, 378, 6
Prévot, M. L., Lequeux, J., Maurice, E., Prévot, L., & Rocca-Volmerange, B. 1984, A&A, 132, 389
Purcell, E. M. 1969, ApJ, 158, 433
Puget, J. L., & Léger, A. 1989, ARA&A, 27, 161
Rieke, G. H., & Lebofsky, M. J. 1985, ApJ, 288, 618
Savage, B. D. 1975, ApJ, 199, 92
Savage, B. D., & Mathis, J. S. 1979, ARA&A, 17, 73
Seaton, M. J. 1979, MNRAS, 187, 73P
Stein, W. A., & Soifer, B. T. 1983, ARA&A, 21, 177
van de Hulst, H. C. 1949, Rech. Astron. Obs. Utrecht., Vol. 11, Part 2
Wolfe, A. M. 1990, in The Interstellar Medium in Galaxies, ed. H. A. Thronson & J. M. Shull (Dordrecht: Kluwer), 387
Wright, E. L. 1990, ApJ, 353, 411